Revision 1

Effect of water on carbonate-silicate liquid immiscibility in the system $KAlSi_3O_8$-$CaMgSi_2O_6$-$NaAlSi_2O_6$-$CaMg(CO_3)_2$ at 6 GPa: implications for diamond-forming melts

Anton Shatskiy[1,2*], Anton V. Arefiev[1,2], Ivan V. Podborodnikov[1,2], Konstantin D. Litasov[3,4]

[1]Sobolev Institute of Geology and Mineralogy, Russian Academy of Science, Siberian Branch, Novosibirsk 630090, Russia

[2]Novosibirsk State University, Novosibirsk 630090, Russia

[3]Vereshchagin Institute for High Pressure Physics, Russian Academy of Science, Troitsk, Moscow, 108840, Russia

[4]Fersman Mineralogical Museum, Russian Academy of Science, Moscow, 115162, Russia

*telephone/fax: +7 (382)-330-75-01, e-mail: shatskiy@igm.nsc.ru

Abstract

To clarify the effect of water on carbonate-silicate liquid immiscibility in the diamond stability field, we performed experiments in the system $KAlSi_3O_8$-$CaMgSi_2O_6$-$NaAlSi_2O_6$-$CaMg(CO_3)_2$ under nominally dry and hydrous conditions with adding 1.5 wt% H_2O at a pressure of 6 GPa and temperatures of 1000 to 1500 °C. Both systems start to melt at 1050-1100 °C. Under anhydrous condition the melting occurs via the following reaction: $6KAlSi_3O_8$ (K-feldspar) + $6CaMg(CO_3)_2$ (dolomite) = $2(Ca_n,Mg_{1-n})_3Al_2Si_3O_{12}$ (garnet) + Al_2SiO_5 (kyanite) + $11SiO_2$ (coesite) + $3K_2(Ca_{1-n},Mg_n)_2(CO_3)_3$ (carbonatitic melt) + $3CO_2$ (fluid and/or liquid), where n ~ 0.3−0.4. The carbonatitic melt has the following composition $38(K_{0.92}Na_{0.08})_2CO_3 \cdot 62Ca_{0.62}Mg_{0.38}CO_3$. A second immiscible silicic melt containing (in wt%, volatile free) SiO_2 = 68.8, Al_2O_3 = 12.6, CaO = 3.7, MgO = 2.4, Na_2O = 1.1, K_2O = 11.3 appears

at 1250 °C. Both melts remain stable up to 1500 °C and coexist with the clinopyroxene ± garnet ± coesite residue assemblage. In the presence of water stored away in phengite, the melting begins from silicic melt, which contains (in wt%, volatile free) SiO_2 = 61.4, Al_2O_3 = 15.3, CaO = 4.8, MgO = 3.0, Na_2O = 2.2, K_2O = 13.3 and coexists with phengite, dolomite, clinopyroxene, and coesite. The phengite + dolomite assemblage remains to 1100 °C and disappears at 1200 °C producing two immiscible melts carbonatitic with approximate composition, $19(K_{0.89}Na_{0.11})_2CO_3 \cdot 81Ca_{0.57}Mg_{0.43}CO_3$, and silicic containing (in wt%, volatile free) SiO_2 = 63.3, Al_2O_3 = 15.6, CaO = 4.5, MgO = 3.0, Na_2O = 2.0, K_2O = 11.6. The present results imply, that partial melting of continental material subducted to a depth of 200 km can yield simultaneous formation of two immiscible melts, K-dolomitic and K-aluminosilicate. Under dry conditions, carbonatitic melt appears earlier (at a lower temperature). Given the low density and high mobility of this melt, it must quickly percolate upward, leaving a refractory eclogite-like residue and leaving no chance for the formation of a second aluminosilicate melt. However, under hydrous conditions silicate melt appears earlier than carbonatitic melt, leaving a phengite- and dolomite-bearing residue, which finally yields the formation of two immiscible silicic and carbonatitic melts. The compositions of these melts fall in the compositional range of carbonatitic and silicic HDFs in diamonds worldwide. Thus, we suggest that the presence of water is a necessary requirement for the formation of immiscible HDFs inclusions in diamonds and this suggestion is strongly supported by natural data from HDFs.

Keywords: carbonate-silicate liquid immiscibility, K-feldspar, phengite, carbonated pelites, high-density fluids, diamond formation, high-pressure experiment, Earth's upper mantle.

Introduction

Compositions of inclusions in diamonds from kimberlites worldwide indicate that highly-potassic carbonatitic and silicic melts/fluids, so-called high-density fluids (HDFs), have existed

at the base of the continental lithosphere during the most of the Earth's history (Smith et al. 2012; Shirey et al. 2013). HDFs are believed to be responsible for mantle metasomatism and the formation of the lithospheric diamonds (Navon et al. 1988). Unlike peridotite- or eclogite-derived melts (Yaxley and Brey 2004; Dasgupta and Hirschmann 2007; Brey et al. 2008), HDFs are characterized by abnormally high concentrations of alkalis, especially potassium (Bulanova et al. 1988; Navon et al. 1988; Novgorodov et al. 1990; Schrauder and Navon 1994).

It was recently found that potassic aluminosilicate and potassic-dolomitic melts, similar to silicic and carbonatitic HDFs in diamonds, are immiscible and can be formed by partial melting of carbonated pelites at 6 GPa (Shatskiy et al. 2019). However, the anhydrous pelite melting begins from a potassic-dolomitic melt at 1000 °C whereas a potassic aluminosilicate melt appears 200 °C higher. It is well known that carbonatite melt is very mobile owing to its buoyancy, low viscosity, and excellent wetting properties (Minarik and Watson 1995; Dobson et al. 1996; Hammouda and Laporte 2000; Stagno et al. 2018). Consequently, it must rapidly escape from the subduction plate leaving a K- and volatile-poor eclogite-like residue and therefore leaving no chance for the formation of a silicic melt. Yet, the experiments of Shatskiy et al. (2019) were conducted under nominally anhydrous conditions and therefore leave obscure the role of water. Water is an important component of the silicic HDF, which may extend the stability of the silicic melt to lower temperatures. It was recently found that hydrous silicic fluid constituted by H_4SiO_4 and $H_6Si_2O_7$ (which could have a composition much more complex, with presence of Na+, K+, Ca^{2+}, and Mg^{2+}) is present as submicron films around most typical mineral inclusions in gem-quality diamonds from kimberlites worldwide (Nimis et al. 2016; Nestola et al. 2018; Nestola et al. 2019a; Nestola et al. 2019b). It is therefore interesting to study a principal effect of water on phase relations and liquid immiscibility in the systems modeling phase relations in carbonated pelites at 6 GPa.

Here we present an experimental study of the subsolidus and melting phase relations in the system $KAlSi_3O_8$ + $CaMgSi_2O_6$ + $NaAlSi_2O_6$ + $CaMg(CO_3)_2$ (Kfs + Di + Jd + Dol) under nominally 'dry' and hydrous conditions at 6 GPa and 900−1500 °C.

Experimental techniques

General procedures

All experiments were performed using the 'Discoverer-1500' DIA-type press and a Kawai-type inner stage of anvils at IGM SB RAS in Novosibirsk, Russia. The inner stage consists of eight 26-mm tungsten carbide cubes, "Fujilloy N-05", with 12-mm truncations. ZrO_2 pressure media (OZ-8C, MinoYogyo Co., Ltd (Shatskiy et al. 2010)) were shaped as a 20.5 mm octahedron with ground edges and corners. Pyrophyllite gaskets, 4.0 mm in both width and thickness, were used to seal the compressed volume and support the anvil flanks.

The cell assembly allows simultaneous loading up to 16 cylindrical samples of 0.9 mm in both diameter and height in a single run (Shatskiy et al. 2018). The sample temperature was measured by a $W_{97}Re_3$-$W_{75}Re_{25}$ thermocouple and controlled automatically within 2.0 °C of the desired value. No correction of the effect of pressure on emf was applied. The maximum temperature gradients within the sample charge were estimated to be from 5 to 8 °C/mm as temperature increases from 1000 to 1500 °C, respectively (Shatskiy et al. 2013). High-temperature pressure calibration was carried out using known phase transitions in SiO_2 (quartz-coesite) (Hemingway et al. 1998) and in $CaGeO_3$ (garnet-perovskite) (Ono et al. 2011). Uncertainty in the temperature and pressure is less than 20 °C and 0.5 GPa, respectively (Shatskiy et al. 2018).

Starting materials

Reagent grade oxides, carbonates, $Ca(OH)_2$, and natural magnesite (<0.1% impurity) and dolomite (<0.3% impurity) from Brumado (Bahia, Brazil), synthetic $NaAlSi_2O_6$ and $CaMgSi_2O_6$ glasses, and synthetic $CaSiO_3$ wollastonite were used to prepare starting mixtures. The starting

materials were blended in an agate mortar with acetone and loaded as a powder into graphite capsules. The loaded capsules were dried at 300 °C for 1–2 h. Prepared assemblies were stored at 200 °C in a vacuum for ≥12 h prior to the experiment. All experiments were conducted at 15-35 % indoor humidity.

Preparation of experimental samples

Since the samples are highly hygroscopic, their preparation requires special care. To avoid the sample damage by atmospheric humidity, we minimized the residence time of the samples on air and used anhydrous lubricants to polish them like that reported by Arefiev et al. (2019a) and Shatskiy et al. (2019).

Analytical procedures

Recovered samples were studied using a MIRA 3 LMU scanning electron microscope (Tescan Orsay Holding) coupled with an INCA energy-dispersive X-ray microanalysis system 450 equipped with the liquid nitrogen-free Large area EDS X-Max-80 Silicon Drift Detector (Oxford Instruments Nanoanalysis Ltd) at IGM SB RAS (Lavrent'ev et al. 2015). Energy-dispersive X-ray (EDX) spectra were collected by using an electron beam-rastering method, in which the stage is stationary while the electron beam moves over the surface area, with dimensions 5-50 μm (for mineral phases) and 50-500 μm (for a quenched melt) at 20 kV accelerating voltage and 1.5 nA beam current. Live counting time for X-ray spectra was 20 s. In the case of low-contrast buck scattered electron (BSE) images, we used element mapping mode combining X-ray intensities of the selected elements (up to three).

Raman measurements were performed using a Horiba Jobin Yvon LabRAM HR800 Raman microspectrometer with the 532-nm Nd:YAG solid-state laser at IGM SB RAS. Spectra were recorded at ambient conditions in backscattering geometry with a laser power of about 1 mW and a spectral resolution of approximately 2 cm^{-1}.

Experimental results

The system $KAlSi_3O_8$ + $CaMgSi_2O_6$ + $NaAlSi_2O_6$ + $CaMg(CO_3)_2$

The results of the experiments are summarized in Table S1. The mass balance calculations are given in Table S2 in mol% and Table S3 in wt%. The compositions of melts, clinopyroxene, and garnet are presented in Table S4. The BSE images of selected samples are shown in Fig. 1. See the nomenclature section for abbreviations.

In run no. D070 (900 °C, 96 h), the sample consists mostly of unreacted components of the starting mixture: $CaMg(CO_3)_2$ (Dol) + $CaMgSi_2O_6$ (Di) + $NaAlSi_2O_6$ (Jd) + $KAlSi_3O_8$ (Kfs). Kfs is partially replaced by Wad + Ky + Coe.

The subsolidus assemblage established at 1000 °C (run no. D070, 96 h) is mainly represented by Kfs, Cpx, and Dol (Figs. 1a, 2a, Tables S2, S3). The Kfs grains contain numerous submicrometer inclusions of Al_2O_3-poor, SiO_2- and K_2O-rich phase, presumably Wad (Fig. 1a). Kfs grains are surrounded by a three-phase aggregate of Wad, Ky and Coe (Fig. 1a). The small grain size allows only semiquantitative analysis of phases in this run. Cpx is represented by the $Di_{51}Jd_{38}En_3Ts_8$ solid solution and has slightly higher Ca# (52 mol%) than dolomite (Ca# = 48 mol%) (Fig. 3, Table S4).

At 1050 °C (run no. D026, 96 h), the LT sample side consists of the Cpx + Dol + Kfs + Mgs aggregate, whereas the Cpx + Coe + Kfs + Ky + L(C) assemblage appears at the HT sample side (Fig. 1b-d). The Cpx composition is $Di_{47}Jd_{41}En_4Ts_8$ (Fig. 3, Table S4). L(C) quenches to a dendritic intergrowth of carbonates and appears in the interstitial space within the Cpx + Kfs + Coe + Ky matrix (Fig. 1d). In molar proportions, an approximate composition of L(C) is $38(K_{0.92}Na_{0.08})_2CO_3 \cdot 62Ca_{0.62}Mg_{0.38}CO_3$ + 3.1 mol% SiO_2 + 1.1 mol% Al_2O_3 (Fig. 4, Table S4).

As temperature increases to 1100 °C (run no. D078, 47 h), Kfs disappears, the Dol fraction decreases, and the Mgs fraction slightly increases (Fig. 2a). The LT sample side consists of Cpx, Coe, Dol, Mgs, and Ky (Fig. 1e, f), whereas the HT side contains Cpx, Coe, and L(C) (Fig. 1e, g).

153 At 1150 °C (run no. D031, 48 h), Dol and Mgs are completely consumed by the melting
154 reaction and the L(C) fraction increased (Fig. 2a, Tables S2, S3). L(C) forms a separate pool
155 adjacent to the HT capsule side (Fig. 1h, i). Well-shaped Grt and Coe crystals appear at the
156 contact with the L(C) pool (Fig. 1h, i). Some Grt crystals are suspended in the melt (Fig. 1i). The
157 LT sample side consists of Cpx, Coe, Grt and a minor amount of Ky (Fig. 1h). Grt is represented
158 by the $Prp_{74}Grs_{26}$ solid solution (Fig. 5, Table S4). Mass balance calculations indicate the
159 formation of molecular CO_2 as melting begins (Fig. 2a, Tables S2, S3).
160 At 1250 °C (run no. D038, 25 h), the L(C) fraction slightly increases, whereas the fractions
161 of Cpx, Coe, and Grt decrease and Ky completely disappears (Fig. 2a). Besides, L(S), containing
162 (in wt%) 64 SiO_2, 12 Al_2O_3, 2 MgO, 4 CaO, 1 Na_2O, 11 K_2O, and 7 CO_2 (Table S4), appears in
163 the interstitial space within the Cpx matrix (Fig. 1j, k).
164 With further temperature increase to 1350 °C (run no. D027, 24 h) and 1500 °C (run no.
165 D028, 6 h), the fraction of L(S) increases, while the fractions of Cpx and L(C) decrease (Fig. 2a,
166 Tables S2, S3). L(S) forms a separate pool sandwiched by L(C) and residue phases (Fig. 1l-o).
167 The rounded blebs of L(C) can be also seen within the silicate glass and the Cpx ± (Grt + Coe)
168 matrix (Fig. 1l, m, o). Grt and Coe completely disappear at 1500 °C (Figs. 2a, 1n, o).
169 As temperature increases from 1050 to 1500 °C, the SiO_2 content in L(C) increases from 3
170 to 9 mol%, whereas K_2O decreases from 17 to 5 mol% (Fig. 4a, f, Table S4). The L(S)
171 composition reveals a decrease of the SiO_2 content and an increase of the MgO and CaO
172 contents as temperature increases from 1250 to 1500 °C (Fig. 4a, c, d, Table S4). Above the
173 solidus, the Jd content in Cpx changes insignificantly, while the amount of the En component in
174 Cpx increases (Fig. 3a, c, Table S4).
175
176 ***The system $KAlSi_3O_8$ + $CaMgSi_2O_6$ + $NaAlSi_2O_6$ + $CaMg(CO_3)_2$ + H_2O***
177 The results of the experiments including the run conditions and phase compositions in both
178 mol% and wt% are summarized in Table S5. The mass balance calculations are given in Table

S6 in mol% and Table S7 in wt%. The compositions of L(C), L(S), Cpx, and Grt are presented in Table S8. The BSE images of selected samples are shown in Fig. 6.

At 900 °C (run no. D011, 71 h) and 1000 °C (run no. D016, 96 h), the subsolidus assemblage consists of Cpx, Ph, Coe, and Dol (Figs. 2b, 6a, b, Table S5). Besides a minor amount of Kfs was observed at 1000 °C (Figs. 6b).

The first melt appears at 1100 °C (run no. D015, 48 h) (Fig. 6c). The melt has an aluminosilicate composition (Table S8). L(S) quenches to a glass, which fills interstitial space between euhedral Cpx crystals (Fig. 6c). Coe, Ph, Dol, and Mgs were also established among the run products (Fig. 6c, Table S5).

As temperature increases to 1200 °C, L(C) appears in addition to L(S) (Fig. 2b, 6d, e, Table S5). L(C) forms a separate pool at the HT side, whereas L(S) fills interstitial space between the Cpx crystals (Fig. 6d, e). The LT sample side is mainly represented by Cpx and Coe. Mgs appears as a thin layer attached to the LT capsule end (Fig. 6d). Grt forms well-shaped crystals up to 50 μm in size suspended in the L(C) (Fig. 6e). Besides, the quenched products of L(C) contain graphite, which looks like numerous black worms on the BSE images (Fig. 6d, e). The graphite was also observed in the quenched products of L(C) as separate crystals at 1300 °C (Fig. 6f, g) and as their segregations at the interface with L(S) at 1400 °C (Fig. 6h, i).

At 1300 °C (run no. D013, 49 h), solid carbonates completely disappear and the residual assemblage is represented by Cpx, Grt, and Coe (Figs. 2b, 6f, g). L(S) forms a pool at the HT side, while L(C) appears as irregular-shaped and rounded bubbles within L(S) (Fig. 6f, g).

As temperature increases to 1400 °C (run no. D017, 8 h), the assemblage and the fractions of phases remain the same (Fig. 2b, Tables S6, S7). L(C) forms a separate pool at the HT side. The L(S) pool is adjacent to that of L(C) from the LT side (Fig. 6h, i). Both L(C) and L(S) also appear in the interstitial space and small segregations between residual crystals of Cpx, Grt , and Coe at the LT sample side (Fig. 6h, i).

As temperature increases over the entire temperature range, the Jd content in Cpx decreases, the En and Ts contents increase, while the Di content does not change systematically (Fig. 3). Ca# of Grt decreases as temperature increases (Fig. 5). The melts retain nearly constant composition (Table S8). Among the obvious changes, an increase in the MgO and Na_2O contents and a decrease in the K_2O content of L(C) can be noted (Table S8).

Discussion

According to the previous experimental results on phase relations in 'dry' carbonated pelite, the generation of the first highly potassic dolomitic melt at 6-8 GPa is controlled by melting reactions involving Ca-Mg carbonates (Dol or Arg+Mgs) and K-phases (Kfs or Wad) (Grassi and Schmidt 2011a; Shatskiy et al. 2019). Based on the phase relations established here in the Kfs + Di + Jd + Dol system (Fig. 2a, Table S2), the melting reaction can be approximated as follows:

$$6KAlSi_3O_8\ (Kfs) + 6CaMg(CO_3)_2\ (Dol) = 2(Ca_n,Mg_{1-n})_3Al_2Si_3O_{12}\ (Grt) + Al_2SiO_5\ (Ky) + 11SiO_2\ (Coe) + 3K_2(Ca_{1-n},Mg_n)_2(CO_3)_3\ (L) + 3CO_2\ (F\ and/or\ L), \quad (1)$$

where n ~ 0.3−0.4. Reaction 1 yields redistribution of potassium from K-feldspar to L(C) with approximate composition $38(K_{0.92}Na_{0.08})_2CO_3 \cdot 62Ca_{0.62}Mg_{0.38}CO_3$. The L(C) composition resamples peritectic P^1 in the K_2CO_3-$CaCO_3$-$MgCO_3$ system established between 1050 and 1100 °C and controlled by the reaction $K_2Ca_3(CO_3)_4 + K_2Mg(CO_3)_2 \rightarrow MgCO_3 + L(C)$ (Fig. 7) (Arefiev et al. 2019b).

The established phase relations (Fig. 2b, Table S6) suggest that clinopyroxene does not play a decisive role in the incipient melting. Similar phase relationships and L(C) compositions in the systems Kfs + Di + Jd + Dol and carbonated pelite (DG2) at 6 GPa (Shatskiy et al. 2019) (Figs. 2b, f, 4) indicate that reaction 1 is dominant melting reaction controlling the solidus of the 'dry' carbonated pelite at 6 GPa.

Adding water to the Kfs + Di + Jd + Dol system stabilizes phengite with the expense of K-feldspar (Fig. 2). As temperature increases from 1000 to 1100 °C the phengite fraction decreases by nearly half, which accompanies an appearance of L(S) and increasing the coesite fraction (Fig. 2b). Our observation is in good agreement with the results of Domanik and Holloway (1996) which indicate that phengite melting occurs near 1100 °C at 6 GPa in a pure mica system. Our data are also consistent with the results of Thomsen and Schmidt (2008) who observed the disappearance of phengite and appearance of L(S) at 1100 °C in the system pelite-CO_2-H_2O at 5 GPa. Unlike Thomsen and Schmidt (2008), who observed the disappearance of Ca-Mg carbonate and appearance of immiscible L(C) at 1100 °C, in our study dolomite and phengite retain up to 1100 °C and disappear at 1200 °C yielding an appearance of L(C) (Fig. 2a).

Thus, in presence of water, L(S) can appear even earlier then L(C). L(S) contains (in wt%, volatile free) SiO_2 = 61.4, Al_2O_3 = 15.3, CaO = 4.8, MgO = 3.0, Na_2O = 2.2, K_2O = 13.3 (Table S8) and resembles L(S) coexisting with L(C) in the system pelite-CO_2-H_2O at 5 GPa and 1050-1100 °C (Thomsen and Schmidt 2008; Tsuno et al. 2012) (Table S9).

The composition of immiscible L(C), $21(K_{0.93}Na_{0.07})_2CO_3 \cdot 79Ca_{0.59}Mg_{0.41}CO_3$, resembles that established in equilibrium with L(S) under anhydrous conditions here and in 'dry' carbonated pelite (DG2) system (Shatskiy et al. 2019) (Fig. 4). However, this L(C) is more alkali-rich than that established by Tsuno et al. (2012) in coexistence with L(S) in the pelite-CO_2-H_2O system at 5 GPa and 1050-1100 °C and containing 2-3 mol% $(K, Na)_2CO_3$ (Table S9).

Summarizing all available data on L(C) established in the system pelite-CO_2-H_2O at 5-8 GPa and 1000-1100 °C, we can suggest that the measured L(C) compositions are largely scattered in terms of the $(K,Na)_2CO_3$ content, which varies from 2-3 mol% to 26-36 mol% (Table S9) (Thomsen and Schmidt 2008; Grassi and Schmidt 2011b; Grassi and Schmidt 2011a; Tsuno et al. 2012). Such large variations inside the 100 °C temperature range are more likely associated with the analytical problems rather than reflect the actual compositions of the melts.

Deviation of the composition of L(C) towards low alkalinity can be caused by the following reasons. Carbonate specimens containing K_2CO_3 and Na_2CO_3 are highly hygroscopic and can be easily damaged by atmospheric humidity. Therefore, some alkalis can be lost during sample preparation and polishing. Another reason is the poor stability (evaporation) of alkaline carbonates under a focused electron beam during EPMA analysis (Shatskiy et al. 2017; Arefiev et al. 2019a; Shatskiy et al. 2019).

Incipient melting of carbonated pelite yields L(S) at ≤ 5 GPa and L(C) at ≥ 5 GPa (Thomsen and Schmidt 2008; Grassi and Schmidt 2011b; Tsuno et al. 2012). Heating of carbonated pelite (DG2) at 6 GPa under anhydrous conditions to 1200 ° C, which is 200 ° C above its solidus, is accompanied by the formation of L(S) coexisting with L(C) to at least 1500 °C (Shatskiy et al. 2019) (Fig. 2f). The present results show that the anhydrous analog system Kfs + Di + Jd + Dol behaves in a similar manner (Fig. 2a).

Adding water to this system in an amount slightly less than that required to complete replacement of K-feldspar by phengite lowers the melting temperature of silicate component yielding an appearance of L(S) at 1100 °C (Fig. 2e). The incipient melting does not cause the complete consumption of K-phase and carbonate. The most of phengite and dolomite remains in the residue and disappear only at 1200 °C to produce two immiscible melts, L(S) and L(C) (Fig. 2b, Tables S6, S7). These melts remain stable to at least 1400 °C in coexistence with the Cpx + Grt + Coe residual assemblage. The present results suggest that the immiscibility gap between potassic aluminosilicate and potassic-dolomitic melts does not be affected by a moderate amount of water (Fig. 8a). This immiscibility gap prevents the continuous transition from silicic to carbonatitic melt through fractional crystallization over any reasonable range of geothermal conditions.

Figure 8 illustrates the compositions of the melts obtained in the present study (pink and blue rhombuses, L(S), and circles, L(C)) in comparison with the pelite-derived melts (grey symbols) and inclusions of HDFs in diamonds worldwide (small colored open circles) (see

Shatskiy et al., 2019 and references therein). The obtained L(S) in the present study resembles pelite-derived phonolitic to trachytic melts (Fig. 4) and fall in the compositional range of the silicic HDFs (brown open circles in Fig. 8a). The established L(C) resembles 'low-Mg' (Ca# 40–70) carbonatite inclusions in 'fibrous' diamonds from the Ebelyakh placers of the northeastern Siberian craton (Zedgenizov et al. 2011) and some other localities (e.g., (Logvinova et al. 2019)). However, most carbonatitic HDFs belongs to 'high-Mg' (Ca# 10-40) (green open circles in Fig. 8b) (Klein-BenDavid et al. 2009; Weiss et al. 2009; Zedgenizov et al. 2009). Sokol et al. (2017) found that interaction of pelite-derived 'low-Mg' L(C) with harzburgite at 1200 and 1350 °C yields the wehrlitization reaction, which shifts the L(C) composition from 'low-Mg' to 'high-Mg'.

Implications

The composition of melt inclusions in natural diamonds varies from silicic (phonolite-trachyte) to carbonatitic (K-dolomite) (Bulanova et al. 1988; Navon et al. 1988; Novgorodov et al. 1990; Schrauder and Navon 1994). Our results indicate that the silicic and carbonatitic endmembers are immiscible and can be derived by partial melting of the phengite ± K-feldspar + clinopyroxene + dolomite assemblage at 6 GPa above 1100 °C. The immiscibility between coexisting carbonatitic and silicic melts explains the fractionation of Nb from Ta, or Zr from Hf observed in the trace-element patterns of fibrous and monocrystalline diamonds (Rege et al. 2010). Our results show that water stored away in phengite has a strong influence on the temperature stability of silicic melt, while it does not affect solidus temperature. The presence of water lowers melting temperatures of aluminosilicate components expanding the stability field of silicic melt toward the lower temperature of ≤ 1100 °C. Thus, the immersion of carbonated material of the continental crust into the mantle by subduction slabs or by continental collision could yield simultaneous formation of phonolite-trachytic and K-dolomitic immiscible melts responsible for the formation of lithospheric diamonds.

306

307 **Nomenclature**

308 Coe – coesite, Cpx – clinopyroxene, Di – diopside, Dol – dolomite, En – enstatite, F – CO_2
309 fluid, Grs – grossular, Grt – garnet, Jd – jadeite, Wad – wadeite structured $K_2Si_4O_9$, Kfs – K-
310 feldspar, Ky – kyanite, L(S) – silicic melt, L(C) – carbonatitic melt, Mgs – magnesite, Ph –
311 phengite, Prp – pyrope, Ts - $CaAlSiAlO_6$ tschermakite.

312

313 **Acknowledgments**

314 This study was done on the state assignment of IGM SB RAS. AS was supported by RFBR
315 No. 20-05-00811. AVA was supported by RFBR No. 19-35-90082. KDL was supported by the
316 state assignment of IHPP RAS. The SEM and EDX studies of experimental samples were
317 performed in the Analytical Center for multi-elemental and isotope research SB RAS. We are
318 grateful to N.S. Karmanov and A.T. Titov for their help in the analytical works.

319

320 **References**

321 Arefiev, A.V., Shatskiy, A., Podborodnikov, I.V., Behtenova, A., and Litasov, K.D. (2019a) The
322 system K_2CO_3–$CaCO_3$–$MgCO_3$ at 3 GPa: Implications for carbonatite melt compositions
323 in the subcontinental lithospheric mantle. Minerals, 9(5), 296.
324 Arefiev, A.V., Shatskiy, A., Podborodnikov, I.V., and Litasov, K.D. (2019b) The K_2CO_3–
325 $CaCO_3$–$MgCO_3$ system at 6 GPa: implications for diamond forming carbonatitic melts.
326 Minerals, 9, 558.
327 Brey, G.P., Bulatov, V.K., Girnis, A.V., and Lahaye, Y. (2008) Experimental melting of
328 carbonated peridotite at 6-10 GPa. Journal of Petrology, 49(4), 797-821.
329 Bulanova, G.P., Novgorodov, P.G., and Pavlova, L.A. (1988) The first find of a melt inclusion in
330 diamond from the Mir pipe. Geokhimia, 756-765 (in Russian).

Dasgupta, R., and Hirschmann, M.M. (2007) Effect of variable carbonate concentration on the solidus of mantle peridotite. American Mineralogist, 92(2-3), 370-379.

Dobson, D.P., Jones, A.P., Rabe, R., Sekine, T., Kurita, K., Taniguchi, T., Kondo, T., Kato, T., Shimomura, O., and Urakawa, S. (1996) In-situ measurement of viscosity and density of carbonate melts at high pressure. Earth and Planetary Science Letters, 143, 207-215.

Domanik, K.J., and Holloway, J.R. (1996) The stability and composition of phengitic muscovite and associated phases from 5.5 to 11 GPa: Implications for deeply subducted sediments. Geochimica et Cosmochimica Acta, 60(21), 4133-4150.

Grassi, D., and Schmidt, M.W. (2011a) Melting of carbonated pelites at 8–13 GPa: generating K-rich carbonatites for mantle metasomatism. Contributions to Mineralogy and Petrology, 162(1), 169-191.

Grassi, D., and Schmidt, M.W. (2011b) The melting of carbonated pelites from 70 to 700 km depth. Journal of Petrology, 52(4), 765-789.

Hammouda, T., and Laporte, D. (2000) Ultrafast mantle impregnation by carbonatite melts. Geology, 28(3), 283-285.

Hemingway, B.S., Bohlen, S.R., Hankins, W., Westrum, E.F., and Kuskov, O.L. (1998) Heat capacity and thermodynamic properties for coesite and jadeite, reexamination of the quartz-coesite equilibrium boundary. American Mineralogist, 83(3-4), 409-418.

Jablon, B.M., and Navon, O. (2016) Most diamonds were created equal. Earth and Planetary Science Letters, 443, 41-47.

Klein-BenDavid, O., Logvinova, A.M., Schrauder, M., Spetius, Z.V., Weiss, Y., Hauri, E.H., Kaminsky, F.V., Sobolev, N.V., and Navon, O. (2009) High-Mg carbonatitic microinclusions in some Yakutian diamonds - a new type of diamond-forming fluid. Lithos, 112(S2), 648-659.

Lavrent'ev, Y.G., Karmanov, N.S., and Usova, L.V. (2015) Electron probe microanalysis of minerals: Microanalyzer or scanning electron microscope? Russian Geology and Geophysics, 56(8), 1154-1161.

Logvinova, A.M., Shatskiy, A., Wirth, R., Tomilenko, A.A., Ugap'eva, S.S., and Sobolev, N.V. (2019) Carbonatite melt in type Ia gem diamond. Lithos, 342-343, 463-467.

Minarik, W.G., and Watson, E.B. (1995) Interconnectivity of carbonate melt at low melt fraction. Earth and Planetary Science Letters, 133(3-4), 423-437.

Navon, O., Hutcheon, I., Rossman, G., and Wasserburg, G. (1988) Mantle-derived fluids in diamond micro-inclusions. Nature, 335(6193), 784-789.

Nestola, F., Prencipe, M., Nimis, P., Sgreva, N., Perritt, S., Chinn, I., and Zaffiro, G. (2018) Toward a robust elastic geobarometry of kyanite inclusions in eclogitic diamonds. Journal of Geophysical Research: Solid Earth, 123(8), 6411-6423.

Nestola, F., Jacob, D.E., Pamato, M.G., Pasqualetto, L., Oliveira, B., Greene, S., Perritt, S., Chinn, I., Milani, S., and Kueter, N. (2019a) Protogenetic garnet inclusions and the age of diamonds. Geology, 47(5), 431-434.

Nestola, F., Zaffiro, G., Mazzucchelli, M.L., Nimis, P., Andreozzi, G.B., Periotto, B., Princivalle, F., Lenaz, D., Secco, L., and Pasqualetto, L. (2019b) Diamond-inclusion system recording old deep lithosphere conditions at Udachnaya (Siberia). Scientific reports, 9(1), 1-8.

Nimis, P., Alvaro, M., Nestola, F., Angel, R.J., Marquardt, K., Rustioni, G., Harris, J.W., and Marone, F. (2016) First evidence of hydrous silicic fluid films around solid inclusions in gem-quality diamonds. Lithos, 260, 384-389.

Novgorodov, P.G., Bulanova, G.P., Pavlova, L.A., Mikhailov, V.N., Ugarov, V.V., Shebanin, A.P., and Argunov, K.P. (1990) Inclusions of potassic phases, coesite and omphacite in the coated diamond crystal from the "Mir" pipe. Dokl Akad Nauk SSSR Earth Sci, 310, p. 439-443.

Ono, S., Kikegawa, T., and Higo, Y. (2011) In situ observation of a garnet/perovskite transition in $CaGeO_3$. Physics and Chemistry of Minerals, 38, 735-740.

Rege, S., Griffin, W.L., Pearson, N., Araújo, D., Zedgenizov, D., and O'Reilly, S.Y. (2010) Trace-element patterns of fibrous and monocrystalline diamonds: Insights into mantle fluids. Lithos, 118(3-4), 313-337.

Schrauder, M., and Navon, O. (1994) Hydrous and carbonatitic mantle fluids in fibrous diamonds from Jwaneng, Botswana. Geochimica et Cosmochimica Acta, 58(2), 761-771.

Shatskiy, A., Litasov, K.D., Terasaki, H., Katsura, T., and Ohtani, E. (2010) Performance of semi-sintered ceramics as pressure-transmitting media up to 30 GPa. High Pressure Research, 30(3), 443-450.

Shatskiy, A., Sharygin, I.S., Gavryushkin, P.N., Litasov, K.D., Borzdov, Y.M., Shcherbakova, A.V., Higo, Y., Funakoshi, K.-i., Palyanov, Y.N., and Ohtani, E. (2013) The system K_2CO_3-$MgCO_3$ at 6 GPa and 900-1450 ºC. American Mineralogist, 98(8-9), 1593-1603.

Shatskiy, A., Podborodnikov, I.V., Arefiev, A.V., Litasov, K.D., Chanyshev, A.D., Sharygin, I.S., Karmanov, N.S., and Ohtani, E. (2017) Effect of alkalis on the reaction of clinopyroxene with Mg-carbonate at 6 GPa: Implications for partial melting of carbonated lherzolite. American Mineralogist, 102(9), 1934-1946.

Shatskiy, A., Podborodnikov, I.V., Arefiev, A.V., Minin, D.A., Chanyshev, A.D., and Litasov, K.D. (2018) Revision of the $CaCO_3$–$MgCO_3$ phase diagram at 3 and 6 GPa. American Mineralogist, 103(3), 441-452.

Shatskiy, A., Arefiev, A.V., Podborodnikov, I.V., and Litasov, K.D. (2019) Origin of K-rich diamond-forming immiscible melts and CO_2 fluid via partial melting of carbonated pelites at a depth of 180-200 km. Gondwana Research, 75(11), 154-171.

Shirey, S.B., Cartigny, P., Frost, D.J., Keshav, S., Nestola, F., Nimis, P., Pearson, D.G., Sobolev, N.V., and Walter, M.J. (2013) Diamonds and the geology of mantle carbon. Rev Mineral Geochem, 75, p. 355-421.

Smith, E.M., Kopylova, M.G., Nowell, G.M., Pearson, D.G., and Ryder, J. (2012) Archean mantle fluids preserved in fibrous diamonds from Wawa, Superior craton. Geology, 40(12), 1071-1074.

Sokol, A.G., Kruk, A.N., Palyanov, Y.N., and Sobolev, N.V. (2017) Stability of phlogopite in ultrapotassic kimberlite-like systems at 5.5–7.5 GPa. Contributions to Mineralogy and Petrology, 172(4), 21.

Stagno, V., Stopponi, V., Kono, Y., Manning, C.E., and Irifune, T. (2018) Experimental determination of the viscosity of Na_2CO_3 melt between 1.7 and 4.6 GPa at 1200–1700° C: Implications for the rheology of carbonatite magmas in the Earth's upper mantle. Chemical Geology, 501, 19-25.

Thomsen, T.B., and Schmidt, M.W. (2008) Melting of carbonated pelites at 2.5–5.0 GPa, silicate–carbonatite liquid immiscibility, and potassium–carbon metasomatism of the mantle. Earth and Planetary Science Letters, 267(1), 17-31.

Tsuno, K., Dasgupta, R., Danielson, L., and Righter, K. (2012) Flux of carbonate melt from deeply subducted pelitic sediments: Geophysical and geochemical implications for the source of Central American volcanic arc. Geophysical Research Letters, 39(16).

Weiss, Y., Kessel, R., Griffin, W.L., Kiflawi, I., Klein-BenDavid, O., Bell, D.R., Harris, J.W., and Navon, O. (2009) A new model for the evolution of diamond-forming fluids: Evidence from microinclusion-bearing diamonds from Kankan, Guinea. Lithos, 112(S2), 660-674.

Yaxley, G.M., and Brey, G.P. (2004) Phase relations of carbonate-bearing eclogite assemblages from 2.5 to 5.5 GPa: implications for petrogenesis of carbonatites. Contributions to Mineralogy and Petrology, 146(5), 606-619.

Zedgenizov, D.A., Ragozin, A.L., Shatsky, V.S., Araujo, D., Griffin, W.L., and Kagi, H. (2009) Mg and Fe-rich carbonate-silicate high-density fluids in cuboid diamonds from the Internationalnaya kimberlite pipe (Yakutia). Lithos, 112(S2), 638-647.

433 Zedgenizov, D.A., Ragozin, A.L., Shatsky, V.S., Araujo, D., and Griffin, W.L. (2011) Fibrous
434 diamonds from the placers of the northeastern Siberian Platform: carbonate and silicate
435 crystallization media. Russian Geology and Geophysics, 52(11), 1298-1309.

436

437

438 **Figure Captions**

439 Figure 1. Representative BSE micrographs of sample cross-sections from experiments in the
440 system $KAlSi_3O_8$ + $CaMgSi_2O_6$ + $NaAlSi_2O_6$ + $CaMg(CO_3)_2$ at 6 GPa. HT and LT – high-
441 temperature and low-temperature sample side, respectively. Abbreviations are given in the
442 nomenclature section. The image g taken in the element mapping mode combining X-ray
443 intensities of the selected elements (K – red and Si – green). (Color online)

444

445 Figure 2. Modal abundances of phases present as a function of temperature in the systems
446 $KAlSi_3O_8$ + $CaMgSi_2O_6$ + $NaAlSi_2O_6$ + $CaMg(CO_3)_2$ (Kfs + Di + Jd + Dol) (a) and $KAlSi_3O_8$ +
447 $CaMgSi_2O_6$ + $NaAlSi_2O_6$ + $CaMg(CO_3)_2$ + 4.9 mol% H_2O (Kfs + Di + Jd + Dol + H_2O) (b) at 6
448 GPa. Modes are in mol% were determined from the bulk compositions of starting mixtures and
449 compositions of phases measured by electron microprobe (Tables S2, S6). Modes in wt% are
450 given in Tables S3, S7). See the nomenclature section for abbreviations. (Color online)

451

452 Figure 3. Variations of jadeite (a), diopside (b), enstatite (c), and $CaAlSiAlO_6$ tschermakite (d)
453 components in clinopyroxene versus temperature in the studied systems at 6 GPa (see Tables S4
454 and S8). The compositions of clinopyroxene from the pelite system (DG2) (Shatskiy et al. 2019)
455 are shown for the comparison. (Color online)

456

457 Figure 4. Carbonatitic, L(C), and silicic, L(S), melts compositions (mol%) as a function of
458 temperature. The compositions are expressed via concentrations of SiO_2 (a), Al_2O_3 (b), CaO (c),
459 MgO (d), Na_2O (e), and K_2O (f). The concentrations are taken from the volatile-bearing
460 compositions normalized to 100 %. The original data are given in Tables S2 and S3 in mol%,
461 and Tables S5 and S6 in wt%. The melts obtained in the system carbonated pelite under
462 nominally dry (DG2) conditions at 6 GPa (Shatskiy et al. 2019) are shown for the comparison.
463 (Color online)

464

465 Figure 5. Variations of Ca# = 100·Ca/(Ca+Mg) in garnet with temperature in the studied systems
466 at 6 GPa. (Color online)

467

468 Figure 6. Representative BSE micrographs of sample cross-sections from experiments in the
469 system $KAlSi_3O_8$ + $CaMgSi_2O_6$ + $NaAlSi_2O_6$ + $CaMg(CO_3)_2$ + 4.9 mol% H_2O at 6 GPa. HT and
470 LT – high-temperature and low-temperature sample side, respectively. The images b and c taken
471 in the element mapping mode combining X-ray intensities of the selected elements (K is marked
472 in red). (Color online)

473

474 Figure 7. Carbonatitic melts established in the present study, plotted on the liquidus projection of
475 the K_2CO_3-$MgCO_3$-$CaCO_3$ system at 6 GPa (Arefiev et al. 2019b). (Color online)

476

477 Figure 8. Compositions (mol%) of carbonatitic – L(C), and silicic – L(S), melts established in
478 the systems Kfs+Di+Jd+Dol±H_2O at 6 GPa and 1000-1500 °C in comparison with HDFs found
479 in diamonds worldwide (e.g., (Navon et al. 1988; Klein-BenDavid et al. 2009; Weiss et al. 2009;
480 Zedgenizov et al. 2009; Jablon and Navon 2016)**.** The original data on HDFs in diamonds and a
481 full list of references are given in Appendix A, Supplementary Tables S7-S10 in (Shatskiy et al.
482 2019). The compositions of melts from the carbonated pelite system (DG2) are from (Shatskiy et
483 al. 2019). (Color online)

484

Kfs+Di+Jd+Dol, 6 GPa Run No.; temperature; run duration

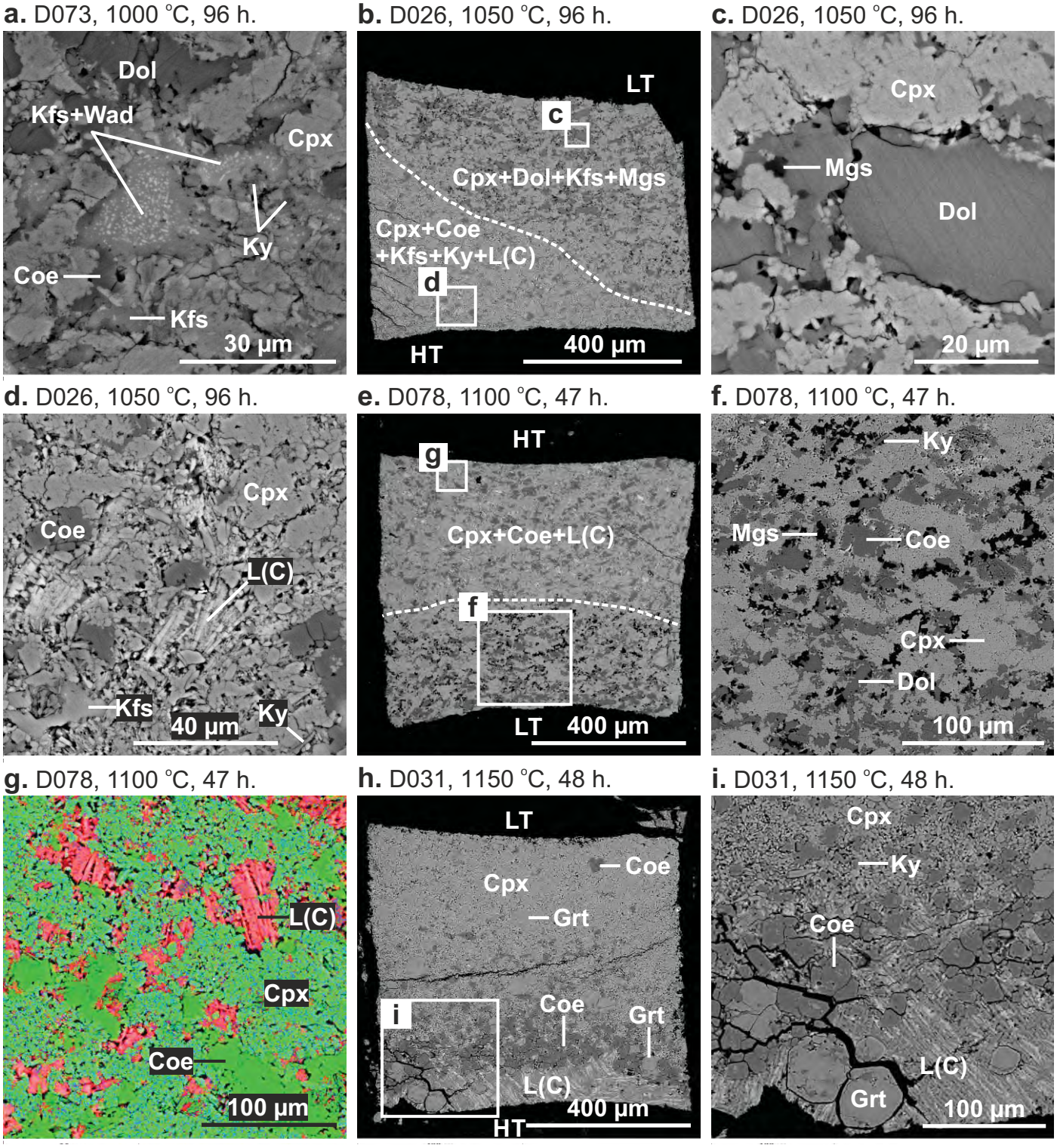

Kfs+Di+Jd+Dol, 6 GPa Run No.; temperature; run duration

j. D038, 1250 °C, 25 h.

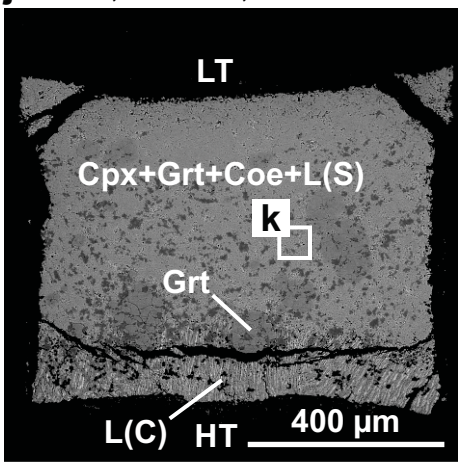

k. D038, 1250 °C, 25 h.

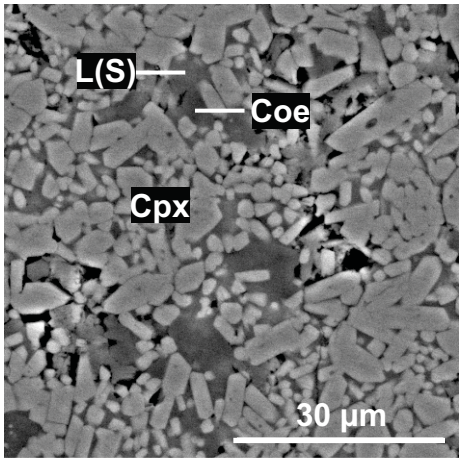

l. D027, 1350 °C, 24 h.

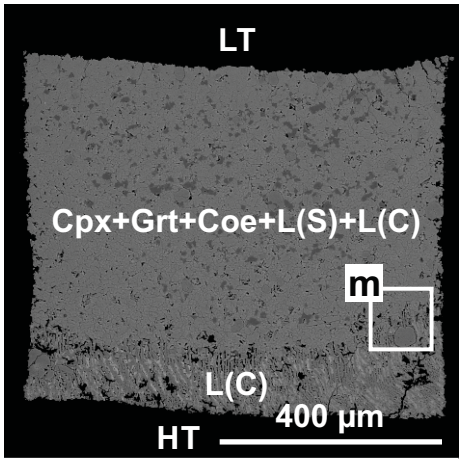

m. D027, 1350 °C, 24 h.

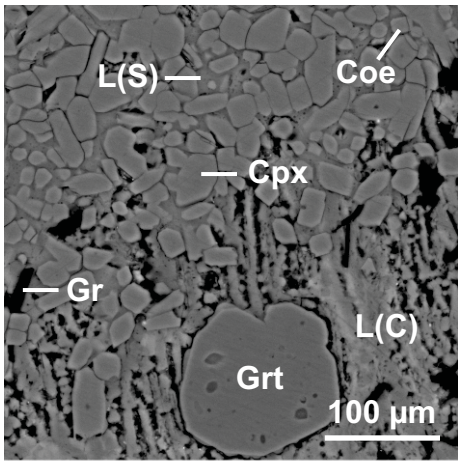

n. D028, 1500 °C, 6 h.

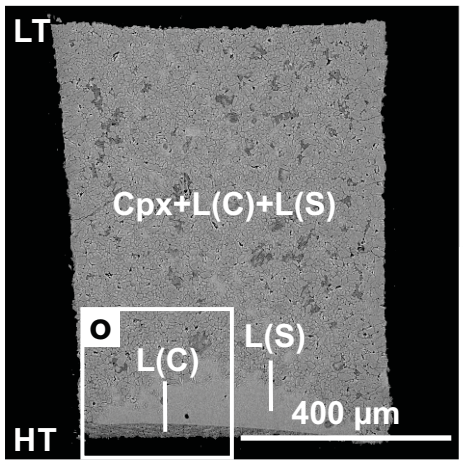

o. D028, 1500 °C, 6 h.

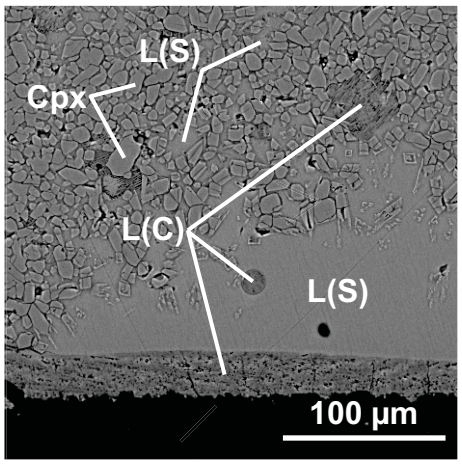

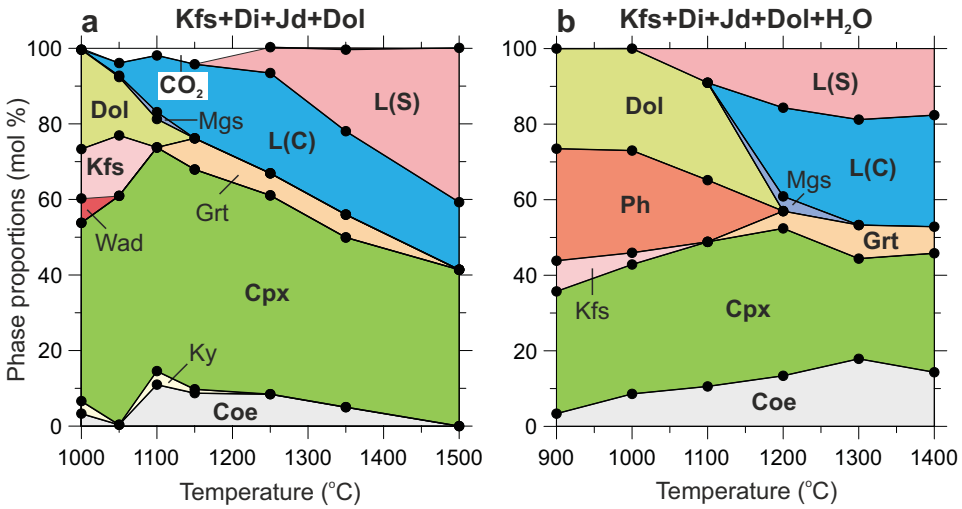
a
Kfs+Di+Jd+Dol
b
Kfs+Di+Jd+Dol+H2O
Phase proportions (mol %)
Temperature (°C)
CO2
Dol
Mgs
L(S)
L(C)
Kfs
Grt
Wad
Cpx
Ky
Coe
Ph

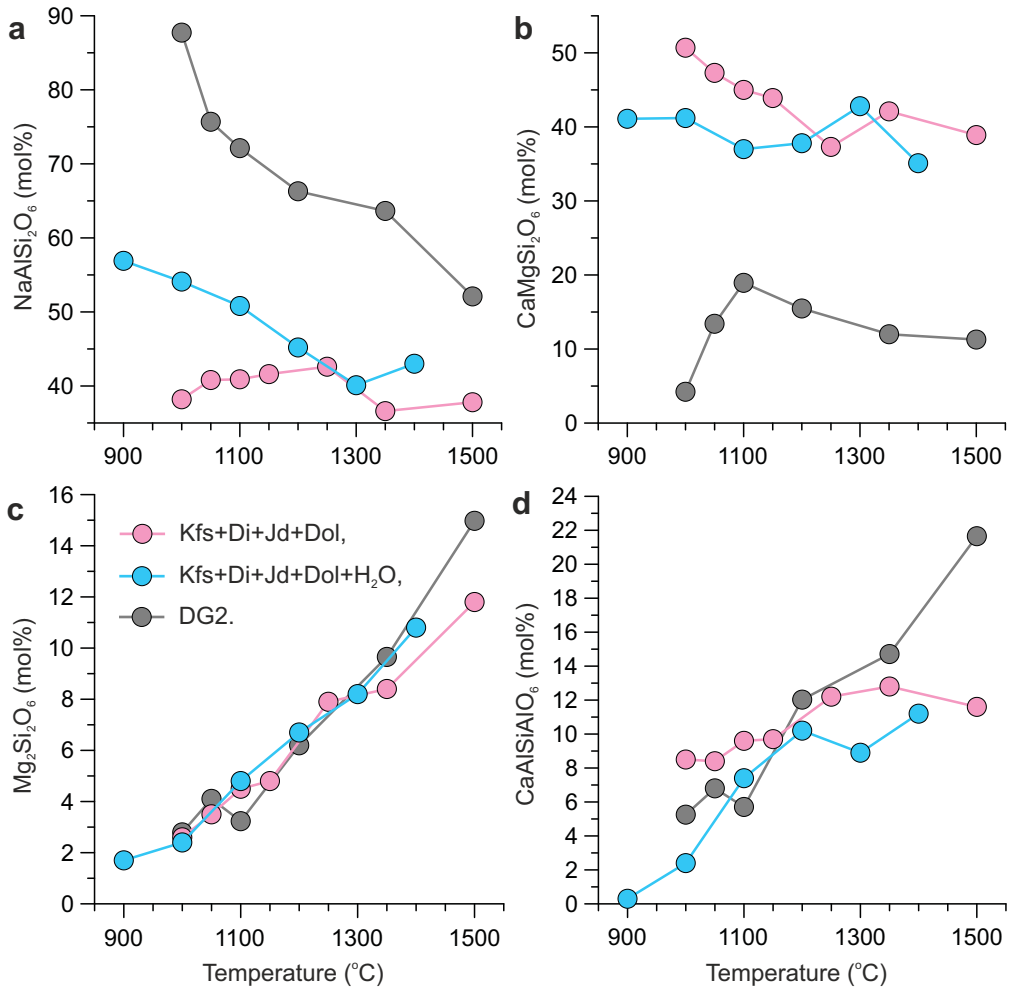
a
b
c
d
NaAlSi2O6 (mol%)
CaMgSi2O6 (mol%)
Mg2Si2O6 (mol%)
CaAlSiAlO6 (mol%)
Kfs+Di+Jd+Dol,
Kfs+Di+Jd+Dol+H2O,
DG2.
Temperature (°C)
Temperature (°C)

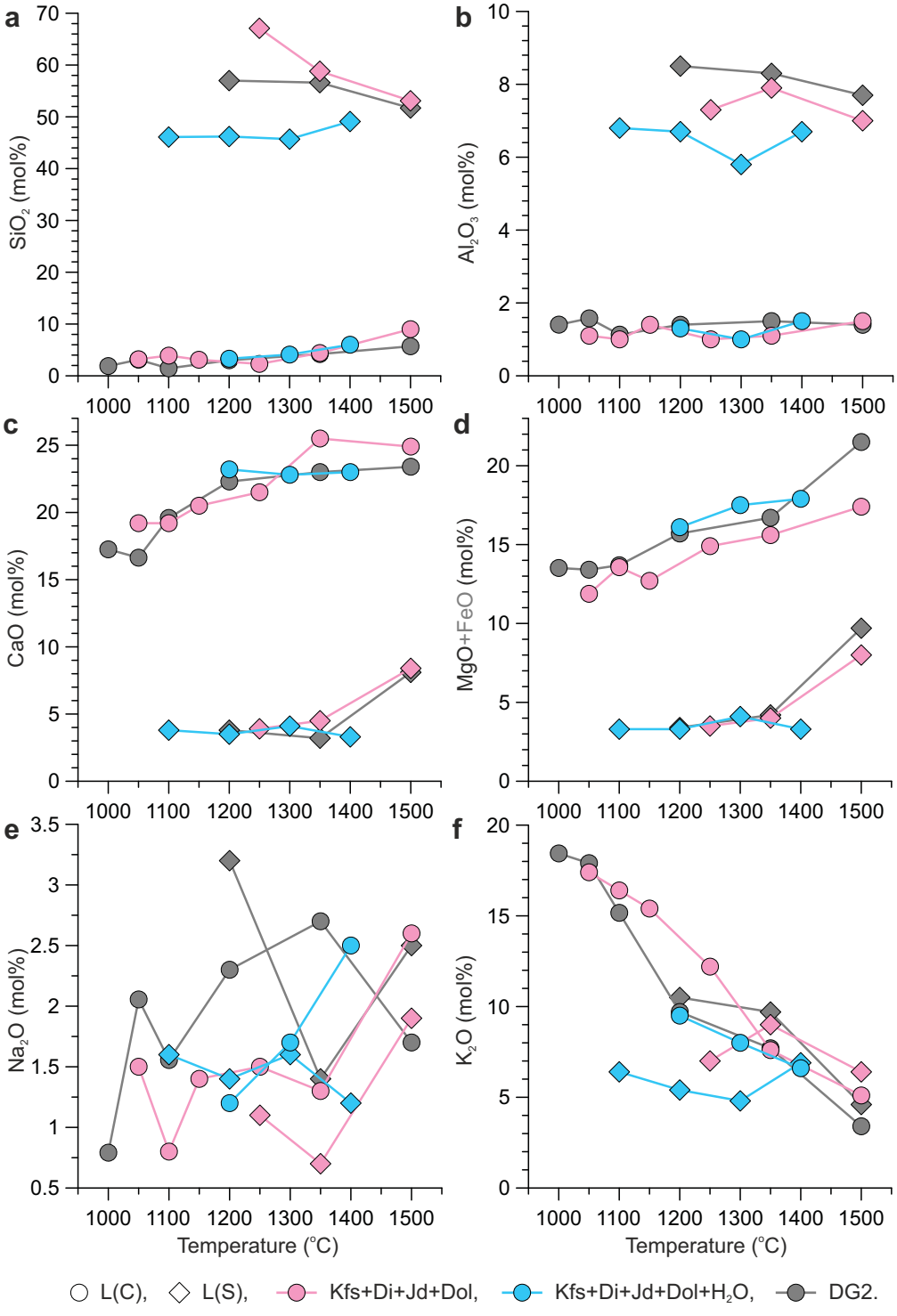
a
b
c
d
e
f
SiO2 (mol%)
Al2O3 (mol%)
CaO (mol%)
MgO+FeO (mol%)
Na2O (mol%)
K2O (mol%)
Temperature (°C)
L(C), L(S), Kfs+Di+Jd+Dol, Kfs+Di+Jd+Dol+H2O, DG2.

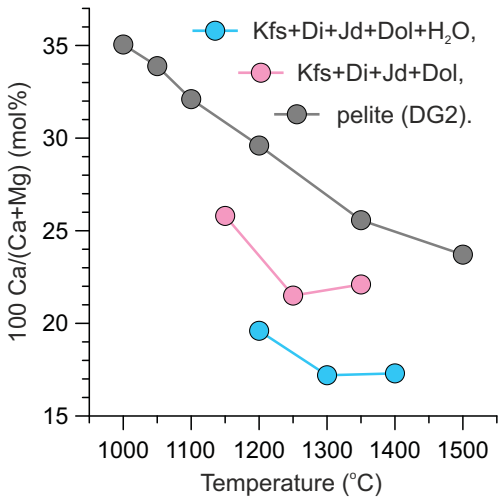
Kfs+Di+Jd+Dol+H2O,
Kfs+Di+Jd+Dol,
pelite (DG2).
100 Ca/(Ca+Mg) (mol%)
35
30
25
20
15
1000
1100
1200
1300
1400
1500
Temperature (°C)

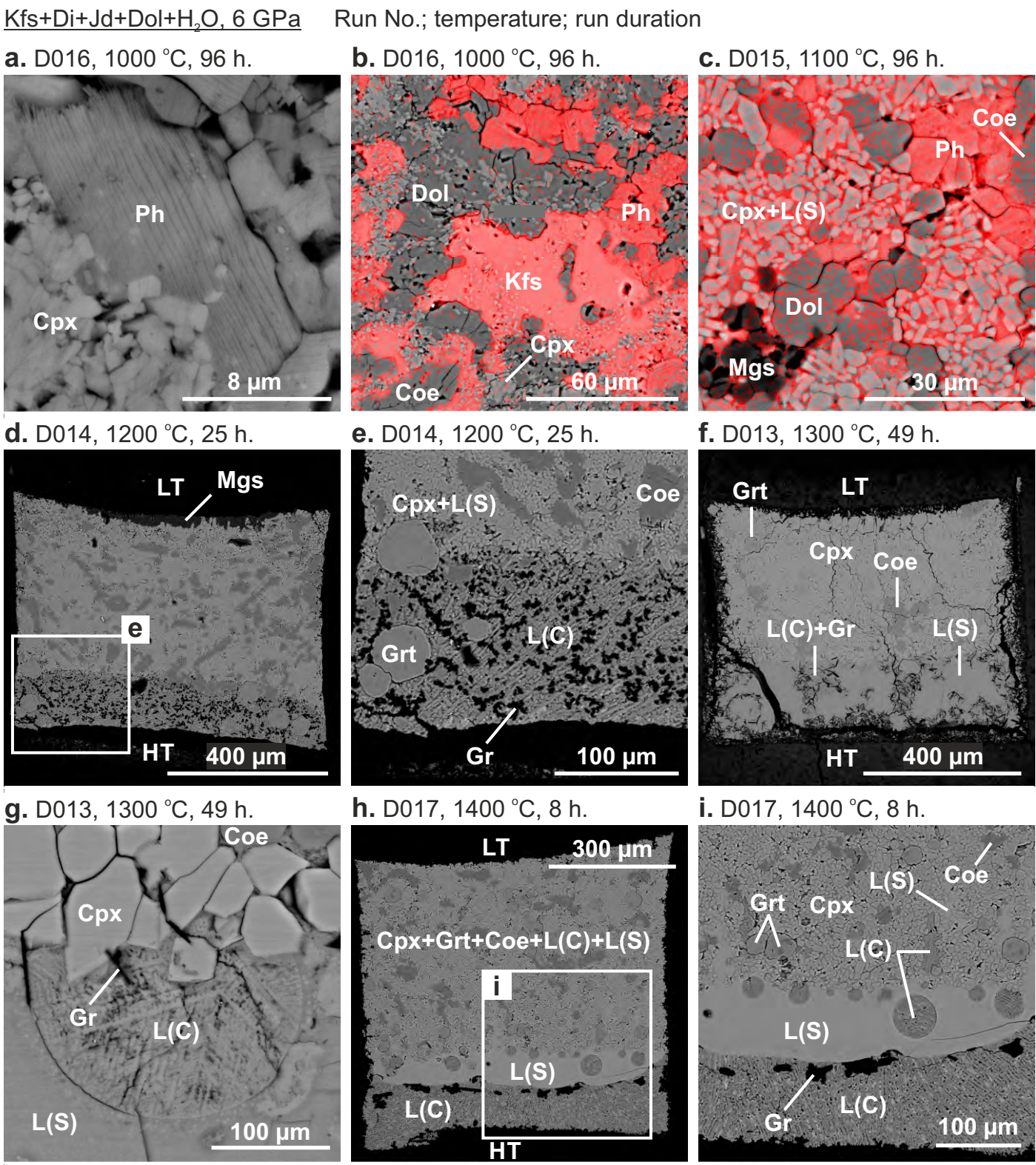
Kfs+Di+Jd+Dol+H2O, 6 GPa
Run No.; temperature; run duration
a. D016, 1000 °C, 96 h.
Ph
Cpx
8 μm
b. D016, 1000 °C, 96 h.
Dol
Ph
Kfs
Cpx
Coe
60 μm
c. D015, 1100 °C, 96 h.
Coe
Ph
Cpx+L(S)
Dol
Mgs
30 μm
d. D014, 1200 °C, 25 h.
LT
Mgs
e
HT
400 μm
e. D014, 1200 °C, 25 h.
Cpx+L(S)
Coe
Grt
L(C)
Gr
100 μm
f. D013, 1300 °C, 49 h.
Grt
LT
Cpx
Coe
L(C)+Gr
L(S)
HT
400 μm
g. D013, 1300 °C, 49 h.
Coe
Cpx
Gr
L(C)
L(S)
100 μm
h. D017, 1400 °C, 8 h.
LT
300 μm
Cpx+Grt+Coe+L(C)+L(S)
i
L(S)
L(C)
HT
i. D017, 1400 °C, 8 h.
L(S)
Coe
Grt
Cpx
L(C)
L(S)
Gr
L(C)
100 μm

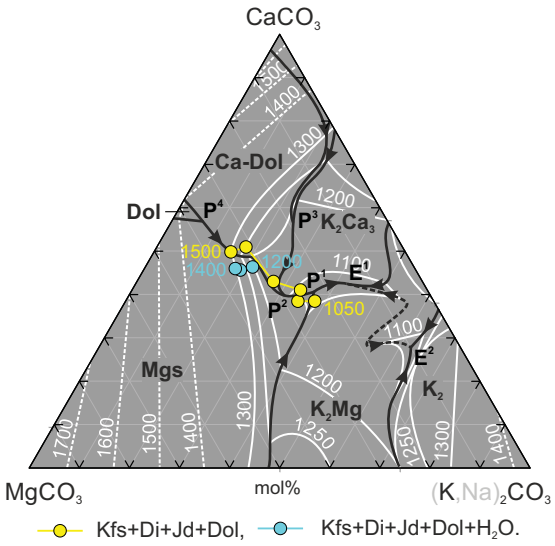
CaCO3
MgCO3
(K,Na)2CO3
mol%
Ca-Dol
Dol
Mgs
K2Mg
K2
P4
P3
K2Ca3
P1
E0
P2
E2
1500
1400
1200
1050
1100
1700
1600
1500
1400
1300
1200
1250
1300
1400
Kfs+Di+Jd+Dol,
Kfs+Di+Jd+Dol+H2O.

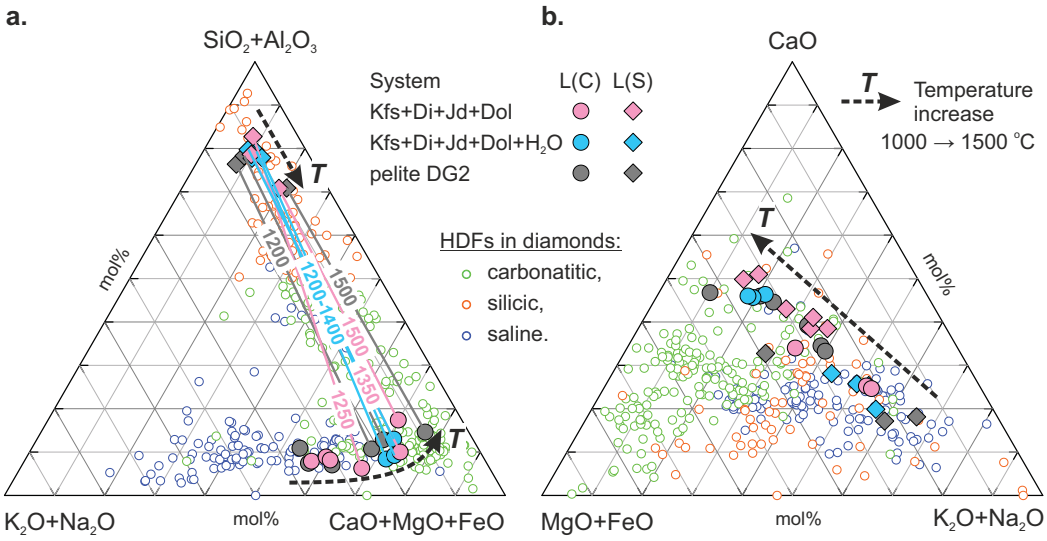
a.
SiO2+Al2O3
K2O+Na2O
mol%
CaO+MgO+FeO
T
1200
1200-1400
1500
1500-1350
1250
System
L(C) L(S)
Kfs+Di+Jd+Dol
Kfs+Di+Jd+Dol+H2O
pelite DG2
HDFs in diamonds:
carbonatitic,
silicic,
saline.
b.
CaO
MgO+FeO
mol%
K2O+Na2O
T
Temperature
increase
1000 → 1500 °C